

1 **Effects of the Three Gorges Dam Operation on the**
2 **hydrological interaction between the Yangtze River and**
3 **downstream aquifers**

4

5 Qi Zhu¹, Ye Kang¹, Zhang Wen^{1*}, Hui Liu¹, Luguang Liu², Yan Li², Xu Li³, Eungyu
6 Park⁴

7

8 1. ¹Hubei Key Laboratory of Yangtze Catchment Environmental Aquatic Science,
9 School of Environmental Studies, China University of Geosciences, Wuhan 430074,
10 Hubei, People's Republic of China

11 2. Hubei Water Resources Research Institute, Wuhan 430070, People's Republic of
12 China

13 3. School of Earth and Environment, Anhui University of Science and Technology,
14 Huainan, People's Republic of China

15 4. Department of Geology, Kyungpook National University, Daegu, Republic of
16 Korea

17

18

19 *Correspondence to: Zhang Wen (wenz@cug.edu.cn)*

20 **Abstract.** The construction of the Three Gorges Dam (TGD) has profoundly altered
21 the groundwater cycle downstream. The obscure spatiotemporal patterns of exchange
22 fluxes between the Yangtze River and groundwater hinder the resolution of water
23 resources and environmental issues in the watershed. This study investigated the
24 spatial extent of the Yangtze River's influence on adjacent groundwater in the Four-
25 Lake Basin, the first river-lake wetland plain downstream of the TGD, using multiple
26 clusters of monitoring wells installed along the river. A coupled SWAT-MODFLOW
27 model was applied to quantify period-specific surface water-groundwater exchanges.
28 A counterfactual scenario without TGD operation, holding other conditions constant
29 is also simulated for comparison. The results show: (1) Under the combined influence
30 of hydrogeological conditions and distance from the TGD, the influence range of the
31 Yangtze River on confined groundwater is significantly greater in the upper section
32 than in the lower section of the Four-Lake Basin, with a difference of approximately
33 one order of magnitude. (2) River and groundwater exchanges exhibit pronounced
34 seasonal and spatial characteristics: river-to-aquifer recharge dominates during
35 drawdown and flooding periods, while aquifer-to-river discharge dominates during
36 impounding and dry periods. Additionally, the interaction rates between river and
37 aquifer are consistently higher in the upper section than in the lower one. (3) Relative
38 to natural conditions, TGD operation dramatically dampens Yangtze River-
39 groundwater interactions overall. The effect is most pronounced during the dry period
40 in the upper section, when the interaction rate decreases by 40.6%. These research
41 outcomes serve as a vital theoretical foundation for assessing the effects of the TGD's
42 regulation on the hydrological interaction in the riparian zone of the Yangtze River.

43 **1 Introduction**

44 High-dam reservoirs play a critical role in flood mitigation, hydroelectric power
45 generation, water supply, and navigation (Poff et al., 1999). To date, approximately
46 50% of rivers worldwide are regulated by dams (Van Cappellen et al., 2016). The
47 dam's impact on the riparian hydrology and biogeochemistry is so pronounced
48 (Palmer and Ruhi, 2019; Song et al., 2020; Maavara et al., 2020) that it can even
49 surpass the effects of hydrological extremes (Dewey et al., 2022). The Three Gorges
50 Dam (TGD), a mega-engineering structure on the mainstream of the Yangtze River,
51 functions as a primary flow regulation structure controlling discharge in the middle
52 reaches. Operational strategies, including early-autumn water impoundment and
53 winter–spring regulated discharge, have substantially altered the river's natural
54 hydrological regime. (Wang et al., 2016; Guo et al., 2022).

55 Centrally located in the Middle Yangtze Basin, the Four-Lake Basin is the first
56 large river-lake wetland system downstream of the TGD. It supports an integrated
57 ecosystem of rivers, lakes, reservoirs, and farmlands (Zhang et al., 2023) and plays a
58 vital role in flood regulation, ecological stabilization, and sustaining agricultural
59 economies (Zhou et al., 2013). However, since the TGD became operational, nitrogen
60 and phosphorus pollution in the water bodies of the middle Yangtze River basin,
61 particularly in areas such as the Four-Lake Basin, has intensified (Gao et al., 2021; Hu
62 et al., 2023; Zhou et al., 2023). While extensive research has documented the impacts
63 of the TGD on the regional water cycle (e.g., Deng et al., 2016; Xiong et al., 2020;
64 Wu et al., 2023), the precise quantification of how TGD-induced river stage
65 fluctuations affect groundwater levels and river-aquifer exchange fluxes, particularly
66 at the basin scale, remains a critical and ongoing challenge.

67 Unlike surface-water-dominated systems, many lakes, rivers, and agricultural
68 wetlands in the Four-Lake Basin interact with the Yangtze mainly through subsurface

69 groundwater exchange (Deng et al., 2016). Yet the extent of the Yangtze's influence,
70 which is a key driver of regional hydrological and ecological processes (Hu et al.,
71 2023; Lai et al., 2025), remains poorly quantified, hindering a clear understanding of
72 groundwater cycling and its ecological consequences. Moreover, TGD operations
73 have introduced significant spatiotemporal variations in water levels along the
74 Yangtze mainstream. Combined with the high spatial heterogeneity of
75 hydrogeological conditions in the riparian zone, these changes complicate efforts to
76 characterize river-groundwater interactions. Although prior research has illuminated
77 local-scale exchange processes (Wang & Wörman, 2019; Huang et al., 2023), such
78 insights are insufficient for assessing basin-wide impacts, underscoring the need for
79 broader monitoring and systematic investigation.

80 Since the TGD's completion, its effects on various downstream ecological
81 components, such as lake levels (Huang et al., 2021), wetland evolution (Zhang et al.,
82 2012), sediment transport (Yang et al., 2007), channel morphology (Sun et al., 2012;
83 Yang et al., 2014), and eco-hydrological conditions affecting vegetation (Xie et al.,
84 2014), have attracted considerable research attention. Nevertheless, the dam's impacts
85 on groundwater systems remains inadequately understood, especially in terms of
86 quantitative attribution isolated from other influencing factors. In the Four-Lake Basin,
87 the presence of an intricate flood-control network further complicates the study of
88 water interactions (World Bank, 2023).

89 While previous quantitative studies have examined hyporheic exchange in the
90 Jiangnan Plain (Du et al., 2018; Jiang et al., 2022), they do not fully account for the
91 compounded effects of hydroclimate, TGD operations, spatial heterogeneity in
92 hydrogeological conditions, and local flood-control and irrigation infrastructure on
93 Yangtze-groundwater interactions in the Four-Lake Basin. To be more precise, in
94 addition to being influenced by the Yangtze River, groundwater levels along the river

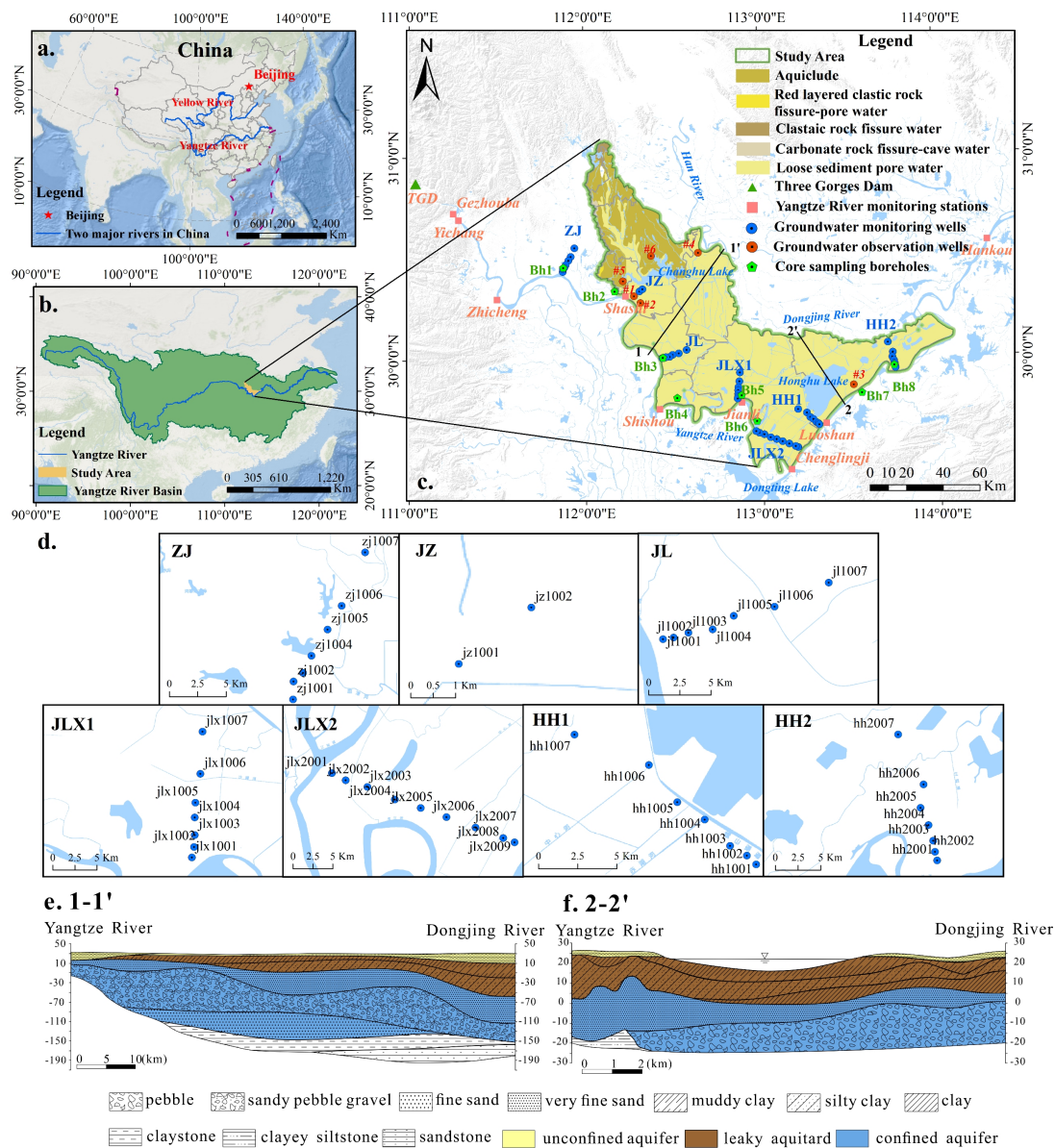
95 are often affected by factors such as runoff generation and concentration, surface soil
96 water infiltration, and recharge from the local surface water network. These factors
97 make traditional groundwater numerical modeling approaches struggle to accurately
98 capture fluctuations in the groundwater table, thereby introducing significant errors in
99 characterizing the exchange processes between the Yangtze River and groundwater.

100 To address these complexities, the SWAT-MODFLOW model offers a robust
101 physically-based framework. This coupled model has been extensively utilized
102 worldwide to simulate complex regional surface water-groundwater (SW-GW)
103 interactions, such as evaluating the effects of agricultural irrigation in the United
104 States (Aliyari et al., 2019), assessing how climate and land-use changes impact
105 groundwater quality in European river basins (Pulido-Velazquez et al., 2015), and
106 analyzing nutrient transport in large river basins in China (Yang et al., 2024).
107 Obviously, for the Sihuan Basin which is distributed with numerous wetlands and water
108 bodies such as rivers, lakes, and paddy fields along the Yangtze River, SWAT-
109 MODFLOW demonstrates high feasibility in characterizing how the groundwater
110 flow system within its complex Quaternary sedimentary formations is influenced by
111 surface terminal water bodies under the regulation of the Three Gorges Reservoir.

112 Aiming to bridge these gaps, this study focuses on the interplay between the
113 Yangtze River and groundwater in the Four-Lake Basin. Data from seven monitoring
114 profiles will be used to identify the spatial influence of the Yangtze River on aquifer
115 dynamics. Based on this influence range, the impact of surface water bodies on
116 groundwater is clearly defined, thereby guiding the development of a field-calibrated
117 SWAT-MODFLOW model to analyze the effects of TGD operations on SW-GW
118 interactions. Ultimately, by constructing a counterfactual scenario without the dam,
119 we aim to isolate and quantify the specific impact of the TGD, providing a
120 quantitative assessment of its influence.

121 **2 Overview of the Study Area**

122 Situated downstream of the TGD on the middle Yangtze's northern bank, the
123 Four-Lake Basin covers an area of about 11,547 km² (Fig. 1). Its boundaries are
124 formed by a combination of natural and artificial features. To the northwest lie the
125 hills of Jingmen and Jiangling counties along with the Zhang River irrigation district;
126 to the north is the watershed of the Han River Basin; and to the east and south, it is
127 bordered by the Yangtze River. The basin's climate is characterized by a mean annual
128 temperature of 15~17 °C, with annual precipitation and evaporation averaging 1,269
129 mm and 1,200 mm, respectively. Located in a flat alluvial plain with an average
130 elevation of 27 m. the Four-Lake Basin features a dense network of interconnected
131 lakes, rivers, and canals, among which Honghu and Changhu Lakes are the most
132 prominent. The Four-Lake Main Channel, as the primary artery of the basin, connects
133 these major lakes and their tributaries, ultimately discharging into the Yangtze River.
134 Groundwater mainly receives combined recharge from precipitation and surface water.
135 Only in a small portion of the northwestern upland areas does groundwater recharge
136 occur predominantly from precipitation, followed by discharge toward the
137 surrounding low-lying plains (Lan et al., 2025; Li et al., 2023). The groundwater table
138 is generally shallow, typically lying 2~5 m below the surface, which facilitates
139 widespread groundwater utilization.



140

141 Figure 1: Map of the study area and monitoring network in the Four-Lake Basin, showing a. the
 142 regional context of the Yangtze River (adapted from the base map in Esri., 2023), b. the basin location
 143 (adapted from the base map in Esri., 2023), c. surface water and groundwater monitoring stations in the
 144 map indicating different types of groundwater, which is entirely compiled according to the internal
 145 survey data from the author's institution, d. groundwater monitoring wells installed along each profile,
 146 e. Stratigraphic profile 1-1' near Jiangling (JL) Profile, and f. Stratigraphic profile 2-2' near Honghu
 147 (HH) Profile.

148 The study area features a groundwater system composed of an unconfined
149 aquifer and multiple confined aquifers. The unconfined aquifer, primarily distributed
150 across the flat central and eastern basin, consists of silty clay, silt, and fine sand, with
151 localized thin gravel layers. Its thickness typically ranges from 3 to 10 m. The upper
152 confined aquifer, which is the most extensive in the region, is composed of clay, silty
153 clay, muddy silty clay, sand, and gravel. Its thickness exhibits considerable spatial
154 variation, generally increasing from the western and peripheral zones toward the
155 central and eastern parts of the basin. In contrast, the lower confined aquifer is
156 predominantly composed of gravel (Huang et al., 2023). Figures 1(e) and 1(f)
157 illustrate the geological cross-sections for profiles 1-1' and 2-2' (locations indicated
158 in Fig. 1c), respectively. From the upstream to the downstream of the basin, the
159 thickness of the clay confining layer increases significantly, while the lithology of the
160 underlying aquifer transitions from highly permeable gravel and pebbles to lower-
161 permeability fine sand.

162 **3 Data and Methods**

163 **3.1 Data Sources**

164 We established a network of groundwater monitoring profiles along the northern
165 bank of the Yangtze River within the Four-Lake Basin, comprising seven distinct
166 profiles-Zhijiang (ZJ), Jingzhou (JZ), Jiangling (JL), Jianli1 (JLX1), Jianli2 (JLX2),
167 Honghu1 (HH1), and Honghu2 (HH2)-with a total of 46 monitoring wells (Fig. 1).
168 Within each profile, wells were systematically positioned at distances of 1, 2, 3, 5, 7,
169 10, 15, 20, and 25 km from the landside toe of the Yangtze River embankment.
170 Groundwater levels were monitored from January 1 to December 31, 2021, at regular
171 5-day intervals. The year 2021 was chosen for investigation due to the availability of

172 a comprehensive dataset from 46 monitoring wells. These wells, arranged in
 173 systematic profiles, provide high spatial density for analyzing lateral water signal
 174 propagation. Additionally, the 5-day monitoring interval is sufficient to capture the
 175 seasonal and operational fluctuations induced by the TGD.

176 The SWAT model primarily required two types of data: spatial data (including
 177 elevation, land use, and soil type data) and meteorological data, with the specific data
 178 formats and sources listed in Table 1. The MODFLOW model necessitated
 179 hydrogeological parameters, recharge and discharge components, and calibration data
 180 derived from long-term groundwater level observations.

181 Table 1 Data types and sources of SWAT model.

Data Type	Data Accuracy	Description	Sources
Digital Elevation Model (DEM)	30 m×30 m	ASTERG DEM V3	Geospatial Data Cloud Platform https://www.gscloud.cn/
Landuse Data	1km×1km	Distribution of land use types	Data Center for Resources and Environmental Sciences https://www.resdc.cn/
Soil Type Data	30m×30 m	Soil type and soil physical properties	Harmonized World Soil Database https://www.fao.org/
Meteorological Data	1/8°×1/8°	Daily average relative humidity, daily cumulative 24-hour precipitation, daily average solar radiation, daily maximum and minimum temperatures, and daily average wind speed	China Meteorological Assimilation Driving Datasets (CMADS V1.2) https://poles.tpdc.ac.cn/

182 The calibration of the MODFLOW model utilized groundwater level data (2011-
 183 2013) obtained from a hydrogeological field investigation conducted in the Jiangnan
 184 Plain during this period (Wen et al., 2017), nearly a decade after the impoundment of
 185 the TGD. To maintain consistency, the same timeframe was adopted for the surface
 186 hydrological modeling data in SWAT to facilitate the model's validation.

187 **3.2 Research Methods**

188 3.2.1 Spatial response analysis of water-level

189 Given that the unconfined aquifer along the Yangtze River is subject to multiple
190 factors, including river stage, precipitation, surface water bodies, and human activities,
191 the water level exhibits frequent fluctuations. This study, therefore, focuses on
192 quantifying the lateral influence of the river on the more stable confined aquifer along
193 its north bank. To this end, water-level data from the confined aquifer were collected
194 through monitoring profiles to investigate the fluctuation patterns of both the river
195 stage and the confined groundwater, as well as the spatial extent of the river's
196 influence. The analytical procedure is detailed below:

197 (1) Data collection and analysis. The river stages and corresponding groundwater
198 levels from the seven monitoring profiles (ZJ, JJ, JL, JLX1, JLX2, HH1, and HH2)
199 with complete 2021 datasets were selected for analysis (Fig. 1). For each month, the
200 daily maximum water level of the Yangtze River was identified, and the
201 corresponding groundwater levels in monitoring wells at various distances were
202 recorded simultaneously. The differences between the maximum water levels of the
203 Yangtze River and groundwater in consecutive months were calculated to derive the
204 fluctuation amplitudes of both at a monthly interval. As shown in the subplot of the
205 ZJ profile in Fig. A1 in the Appendix A, the legend "1/9–2/17" indicates that January
206 9 and February 17 represent the days when the peak water levels of the Yangtze River
207 occurred in their respective months. The difference in water levels between these two
208 days forms the black polyline in the figure. It is important to note that the monthly
209 maximum water level of the Yangtze River was selected because the peak value is the
210 most prominent and objectively identifiable feature, avoiding subjectivity in selecting
211 dates during periods of mild fluctuation. Moreover, the high water level exerts the

212 strongest driving force on the adjacent groundwater, theoretically maximizing the
213 reflection of groundwater response to changes in the Yangtze River water level.

214 (2) Construction and fitting of water-level spatial response equations. A critical
215 step in this analysis was to develop empirical equations that quantify the response of
216 groundwater levels to fluctuations in the Yangtze River stage at different distances
217 from the river. Unlike previous studies, such as Wang and Wörman (2019), which
218 focused mainly on temporal variations in groundwater, the present study employs the
219 analytical solution proposed by Liu et al. (2021) to demonstrate the exponential
220 attenuation of groundwater response amplitudes with distance from the riverbank
221 under sinusoidal river-stage variations, which can be expressed as:

$$222 \quad y = a \cdot e^{bx} \quad (1)$$

223 where y represents the variation amplitude of the groundwater level [m]; x represents
224 the distance from the monitoring point to the riverbank [m]; a represents the change
225 of the Yangtze River water level within a specific period [m]; b represents the
226 attenuation coefficient [1/m]. For each monitoring profile shown in Fig. A1, eleven
227 polylines derived from the monthly water level differences are generated. Then those
228 polylines exhibiting abnormal patterns due to measurement errors or localized
229 hydrological influences are excluded. For each remaining polyline, Eq. (1) is applied
230 for fitting to inversely estimate the corresponding a and b values. The multiple b
231 values from each profile are then averaged to obtain \bar{b} , which is a new profile-
232 specific attenuation coefficient for Eq. (1).

233 (3) Delineation of lateral influence extent. In hydrogeological practice, the
234 intensity of river influence on lateral groundwater dynamics is commonly
235 characterized by a dimensionless parameter R . Here, R is defined as the ratio of the

236 groundwater level fluctuation amplitude to the simultaneous river stage fluctuation
237 amplitude. It signifies the strength of the groundwater response to river fluctuations.

238 Therefore, by reformulating Eq. (1) and substituting the value of \bar{b} obtained from
239 Step (2), the formula for calculating the R value for each monitoring profile can be
240 expressed as

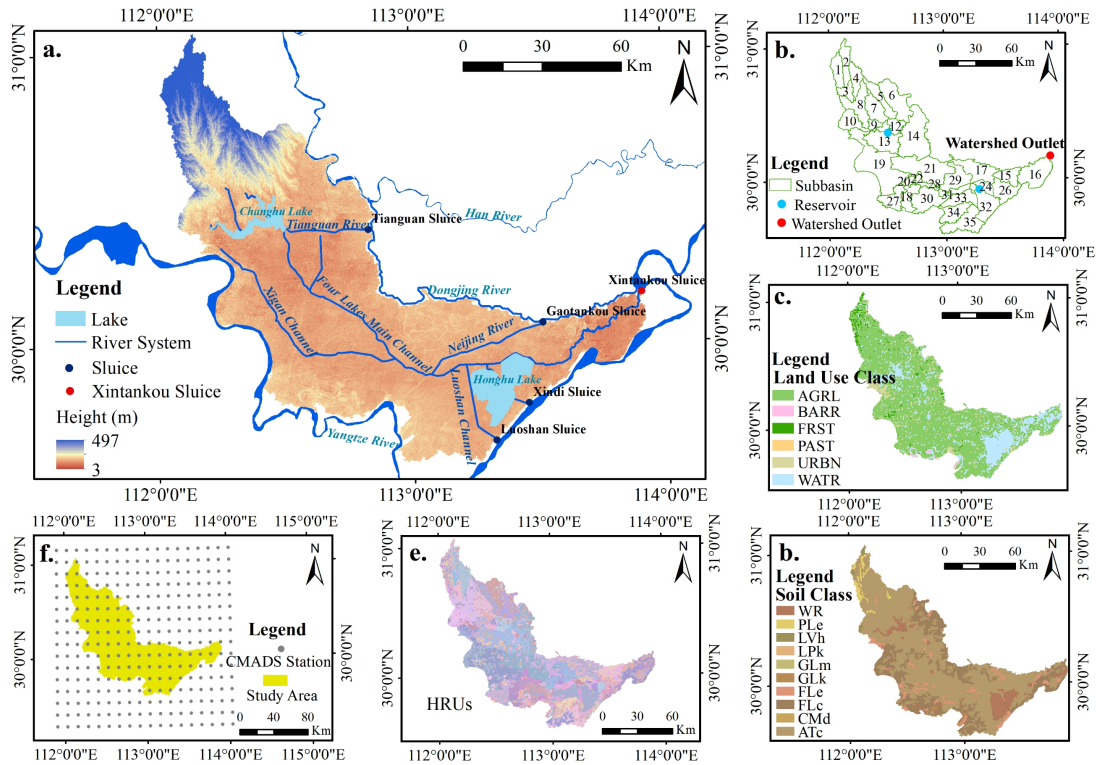
$$241 \quad R = y/a = e^{\bar{b}x} \quad (2)$$

242 According to established criteria (He and Cai, 1999), when $R < 0.02$, i.e., when
243 the groundwater fluctuation falls below 2% of the corresponding river stage
244 fluctuation, the river is considered to have no significant influence on the groundwater.
245 Thus, the distance from the riverbank corresponding to $R = 0.02$ was taken as the
246 maximum lateral influence extent of the Yangtze River on the confined aquifer.
247 Therefore, with the value of \bar{b} obtained in Step (2), the value of x , which indicates the
248 lateral influence range of the Yangtze River on groundwater, can be determined
249 inversely by assigning a value to R .

250 3.2.2 SWAT-MODFLOW coupling model for the Four-Lake Basin

251 After delineating the spatial response range through the data-driven approach,
252 one can clearly identify which surface water bodies, besides the Yangtze River,
253 significantly affect groundwater along the river, justifying the necessity of
254 considering them in a SW-GW interaction framework. The SWAT model for the
255 Four-Lake Basin was developed in ArcSWAT, with all data sources detailed in Table
256 1. The modeling framework began with watershed delineation, dividing the basin into
257 35 subbasins based on Digital Elevation Model (DEM) data and the river network.
258 Hydrologic Response Units (HRUs) were generated by overlaying land use
259 classification, soil types, and slope categories, ultimately producing 428 HRUs as

260 illustrated in Fig. 2. Meteorological data was extracted from the CAMADS v1.2
 261 dataset at 288 monitoring stations within and around the basin (Fig. 2f). The
 262 simulation spanned a three-year warm-up period (2008-2010), followed by calibration
 263 (2011-2014) and validation (2015-2016) phases, all performed at a monthly temporal
 264 resolution.



265
 266 Figure 2: The information of all the basic elements required for constructing the SWAT model: a.
 267 Four-Lake Basin elevations, major water systems, and major sluices. b. SWAT Model subbasins and
 268 watershed outlets. c. Land use classification. d. Soil classification. e. SWAT Model HRUs. f. CAMADS
 269 V1.2 stations.

270 A groundwater numerical simulation using the finite difference method was
 271 performed with Visual MODFLOW Flex 9.0. Based on regional hydrogeological
 272 conditions and borehole lithological data, a heterogeneous, anisotropic, and transient
 273 groundwater flow model for the Four-Lake Basin was generalized into three layers:

274 an unconfined aquifer, an aquitard, and a confined aquifer. The model was discretized
275 horizontally into 1 km × 1 km grids and vertically into three layers based on
276 hydrogeological stratification, resulting in 33,450 active cells. Hydrogeological
277 parameter zones, values, and boundary conditions are detailed in Fig. A2 and Table
278 A1 in the Appendix A.

279 The SWAT-MODFLOW coupled model was developed by establishing a one-
280 way correspondence between SWAT Hydrologic Response Units (HRUs) and
281 MODFLOW grid cells, in which SWAT provides spatially distributed groundwater
282 recharge to MODFLOW, while groundwater feedback to SWAT is not explicitly
283 simulated. This is reasonable because this study aims to investigate the interaction
284 rate between Yangtze River and groundwater instead of delineating the hydrodynamics
285 of surface water; additionally, under the intensive regulation of artificial drainage and
286 irrigation pumping stations in the Four-Lake Basin, the effect of surface water
287 recharge on groundwater is substantially greater than the influence of groundwater
288 discharge on surface water. The calibrated SWAT model provided monthly
289 groundwater recharge (GW_RCHG) and actual evapotranspiration data, which were
290 then assigned to the corresponding MODFLOW cells. These outputs were directly
291 used as inputs for the Recharge (RCH) and Evapotranspiration (EVT) packages in
292 MODFLOW, thereby driving the groundwater flow simulation.

293 **4 Results and Discussion**

294 **4.1 The influence range of the Yangtze River on lateral groundwater**

295 The response of confined groundwater levels to fluctuations in the Yangtze River
296 stage was evaluated across seven monitoring profiles (ZJ, JZ, JL, JLX1, JLX2, HH1,
297 and HH2) at increasing distances (x) from the river. As illustrated in Fig. A1, the

298 sensitivity of groundwater levels to river stage diminishes with distance. One notable
 299 deviation is observed along the ZJ profile, where anomalously large groundwater
 300 fluctuations occur 5 ~ 10 km from the riverbank, possibly due to local
 301 hydrogeological heterogeneity or anthropogenic influences. The amplitude-distance
 302 relationships for both the Yangtze River and groundwater levels, fitted using Eq. (1)
 303 across all seven monitoring profiles, are shown in Fig. A3 in the Appendix A. For
 304 clarity, results from a representative period of the year are displayed. All fitted curves
 305 demonstrate a high goodness-of-fit ($R^2 > 0.9$), indicating highly reliable correlations.
 306 Based on these relationships, the range of estimated b values and the corresponding
 307 fitting equations for each profile were calculated, as summarized in Table 2.

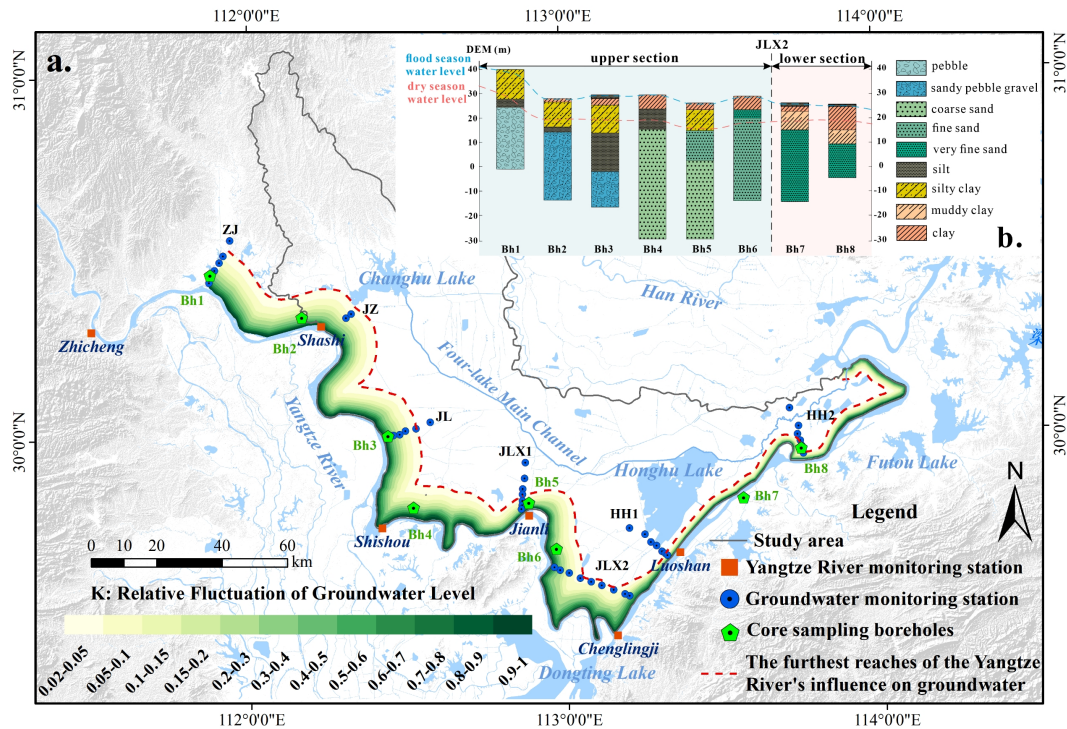
308 Table 2 The range of estimated values of b and corresponding fitting equations for each profile.

Profiles	The range of estimated values of b	Attenuation fitting equation
ZJ	-0.1271~-0.4081	$R_{zj}=e^{-0.3064x}$
JZ	-0.3375~-0.3569	$R_{zj}=e^{-0.3463x}$
JL	-0.3272~-0.4432	$R_{jl}=e^{-0.3687x}$
JLX1	-0.556~-0.8021	$R_{jlx1}=e^{-0.6935x}$
JLX2	-0.2546~-0.5289	$R_{jlx2}=e^{-0.3824x}$
HH1	-1.7839~-2.5305	$R_{hh1}=e^{-2.0203x}$
HH2	-1.4486~-2.0477	$R_{hh2}=e^{-1.7638x}$

309 To quantify the intensity and maximum lateral extent of the Yangtze River's
 310 influence on the adjacent confined aquifer, the criterion defined in step (3) was
 311 applied. According to this criterion, the distance x corresponding to a relative
 312 groundwater fluctuation (R) of 0.02 represents the maximum influence distance.
 313 Table 3 presents the calculated maximum influence distances and the mean
 314 attenuation coefficients (\bar{b}) for each monitoring profile. At the same time, Fig. 3
 315 visually depicts the influence distances across a range of R values, including this
 316 maximum extent.

317 Table 3 Distance x from the riverbank corresponding to $R = 0.02$ and average attenuation coefficient \bar{b}
 318 for each profile.

Profiles	ZJ	JZ	JL	JLX1	JLX2	HH1	HH2
x	12.77	11.30	10.61	5.64	10.23	1.94	2.22
\bar{b}	-0.3064	-0.3463	-0.3687	-0.6935	-0.3824	-2.0203	-1.7638



319
 320 Figure 3: Figure representing the effects of geological conditions on the lateral influences of Yangtze
 321 River on groundwater: a. Different degrees and ranges of influence of the Yangtze River on the lateral
 322 confined groundwater in the Four-Lake Basin. b. Lithologic logs of boreholes along the Yangtze
 323 River in the Four-Lake Basin.

324 As summarized in Table 3 and Fig. 3, the influences of the Yangtze River on the
 325 confined groundwater in the Four-Lake Basin exhibits distinct spatial zoning, with
 326 JLX2 acting as a critical boundary. Consequently, the study area is divided into two
 327 independent segments, i.e., the ZJ-JLX2 reach and the JLX2-HH2 reach, which can
 328 be characterized by three key features:

329 (1) Extended influence range: The ZJ-JLX2 segment shows a smaller attenuation
330 coefficient (b) and a maximum influence distance of 12.77 km (Table 3), indicating
331 more efficient pressure transmission through the aquifer system than in the JLX2-
332 HH2 reach downstream.

333 (2) Hydraulic head differences primarily drive groundwater response: Due to its
334 proximity to the TGD, the ZJ-JLX2 segment experiences amplified river-stage
335 fluctuations that propagate over long distances. In contrast, the JLX2-HH2 segment
336 lies downstream of the Yangtze River after regulation by Dongting Lake, where river
337 stage variations are markedly dampened, leading to a shorter propagation distance of
338 hydraulic signals. Note that the Yangtze River's lateral influence range at the JLX1
339 profile is only 5.64 km, which differs significantly from other cross-sections within
340 the reach. This is because the JLX1 profile is located precisely at the point where the
341 Yangtze River channel bends inward toward the interior of the Four-Lake Basin. The
342 proximity to both the internal water system of the basin and the densely populated
343 area of Jianli City results in a significantly weak response of the JLX1 profile to water
344 level fluctuations in the Yangtze River.

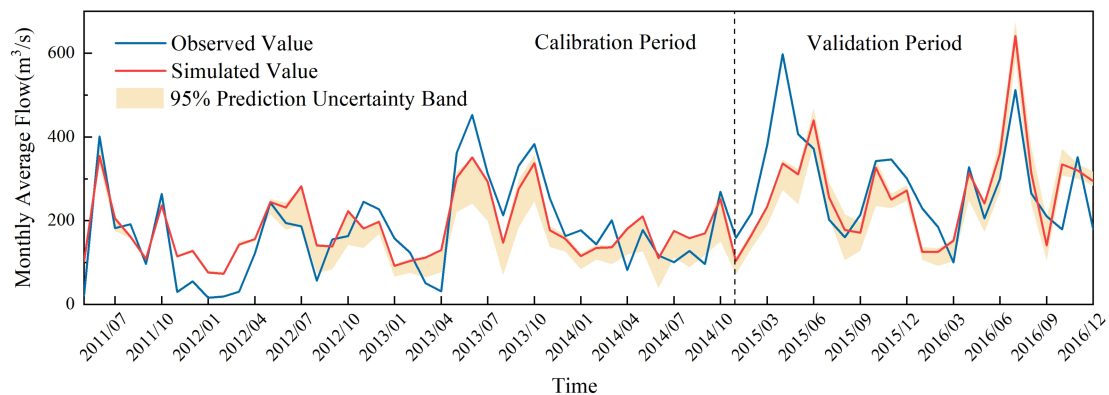
345 (3) Favorable hydrogeological conditions: The JL profile, representative of the
346 ZJ-JLX2 segment, consists of highly permeable gravel-cobble formations (Fig. 1e),
347 which minimize hydraulic head loss and support long-distance transmission of river-
348 induced fluctuations. Although the 2021 Yangtze River Sediment Bulletin indicates
349 that the river incises into the confined aquifer in the JLX2-HH2 segment, Fig. 1f
350 shows that near the profiles HH1 and HH2, the aquifer materials are dominated by
351 fine sands. The resulting lower permeability and higher flow resistance cause rapid
352 attenuation of head fluctuations, thus restricting the lateral extent of the river's
353 influence.

354 Furthermore, the proximity of Honghu Lake to the HH1 and HH2 segment
355 warrants consideration. Although not in direct hydraulic contact with the confined
356 aquifer, this extensive shallow lake interacts dynamically with the overlying phreatic
357 aquifer. As shown in Fig. 1f, the shallow aquitard in the vicinity of Honghu Lake
358 exhibits significant spatiotemporal heterogeneity in thickness, facilitating localized
359 hydraulic connectivity between the unconfined and confined aquifer systems. Under
360 these conditions, Honghu Lake acts as a hydrological buffer; that is, its relatively
361 stable water levels attenuate the transmission of Yangtze River stage fluctuations to
362 adjacent groundwater systems. In addition, we generated the results shown in Fig. 3
363 for the period from 2022 to 2024, and compared the lateral influence range of the
364 Yangtze River on coastal groundwater for each year from 2021 to 2024 (as shown in
365 Fig. A4). The results indicate that this lateral influence range has not changed
366 significantly in recent years, which may be attributed to the fact that annual
367 precipitation in this region has remained consistently between 1000 and 1200
368 millimeters.

369 Based on the analysis of data-driven, the high goodness-of-fit ($R^2 > 0.9$) across
370 all profiles suggests a stable groundwater response to Yangtze River stage
371 fluctuations. Moreover, the derived spatial variation in attenuation coefficients and
372 influence distances is consistent with observed along-river differences in
373 hydrogeological conditions, providing confidence in the robustness of this approach.
374 These results also serve as an independent reference for interpreting the spatial
375 patterns simulated by the coupled SWAT-MODFLOW model in later sections. It is
376 also worth noting that since the establishment of the riparian monitoring network,
377 annual precipitation in the study area has shown limited variability. As a result,
378 findings from years other than 2021 do not differ substantially from those of 2021,
379 which justifies its selection as a representative year in this study.

380 4.2 Validation of the SWAT-MODFLOW model

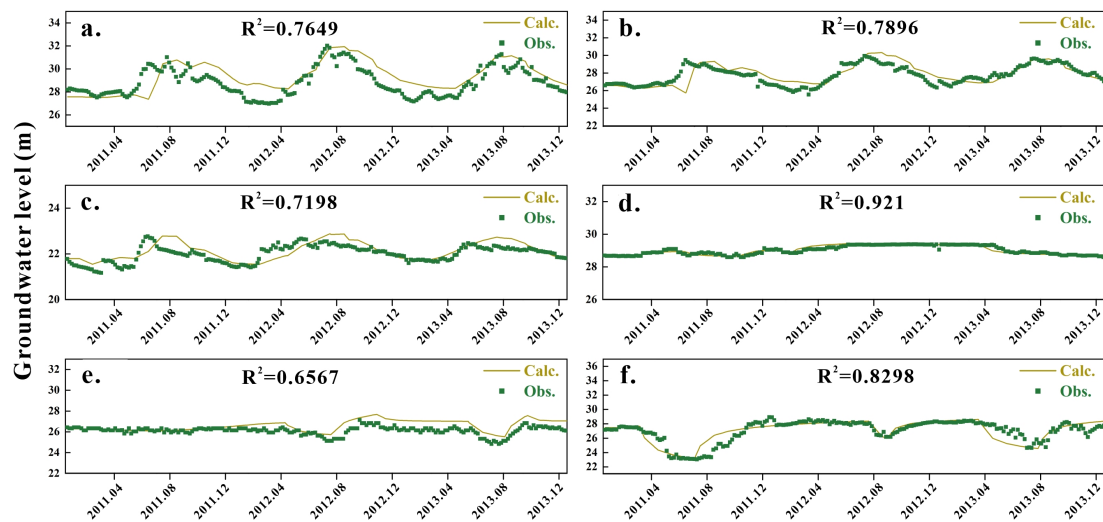
381 Clearly, the results in Section 4.1 demonstrate that the lateral influence range of
382 the Yangtze River encompasses various surface water bodies, highlighting the
383 necessity of using the SWAT-MODFLOW model. The SWAT model for the Four-
384 Lake Basin was calibrated and evaluated using SWAT-CUP, a dedicated tool for
385 parameter calibration and uncertainty analysis for SWAT model. Sensitivity analysis,
386 a key step within this process, was conducted with the SUFI-2 algorithm to identify
387 the parameters exerting the greatest influence on the model outputs (Khaleghi et al.,
388 2024). A total of 17 key parameters were selected for sensitivity analysis and
389 calibration, with 1,000 iterations conducted to optimize model performance. Table A2
390 summarizes the calibrated parameters, their fitted values, and sensitivity ranks.
391 Monthly surface runoff data from the Xintankou station (outlet of sub-basin 16) from
392 2011 to 2016 were used for both model calibration (2011-2014) and validation (2015-
393 2016). As shown in Fig. 4, the model performed well, achieving Nash-Sutcliffe
394 efficiency (NSE) values of 0.7 and 0.65 during calibration and validation, respectively,
395 and R^2 values of 0.76 (calibration) and 0.67 (validation), indicating satisfactory
396 agreement between simulated and observed runoff.



397

398 Figure 4: The fitting between the simulated monthly flow that has been calibrated and the observed one.

399 The coupled SWAT-MODFLOW model was calibrated against observed
 400 groundwater levels from six monitoring wells from 2011 to 2013 distributed near
 401 Yangtze River (Fig. 1). As shown in Fig. 5, the simulated groundwater levels agree
 402 well with the observed values throughout the simulation period, demonstrating the
 403 capability of the model to reproduce regional groundwater dynamics. These results
 404 confirm that the integrated model reliably captures the key characteristics of surface
 405 water-groundwater interactions in the Four-Lake Basin.

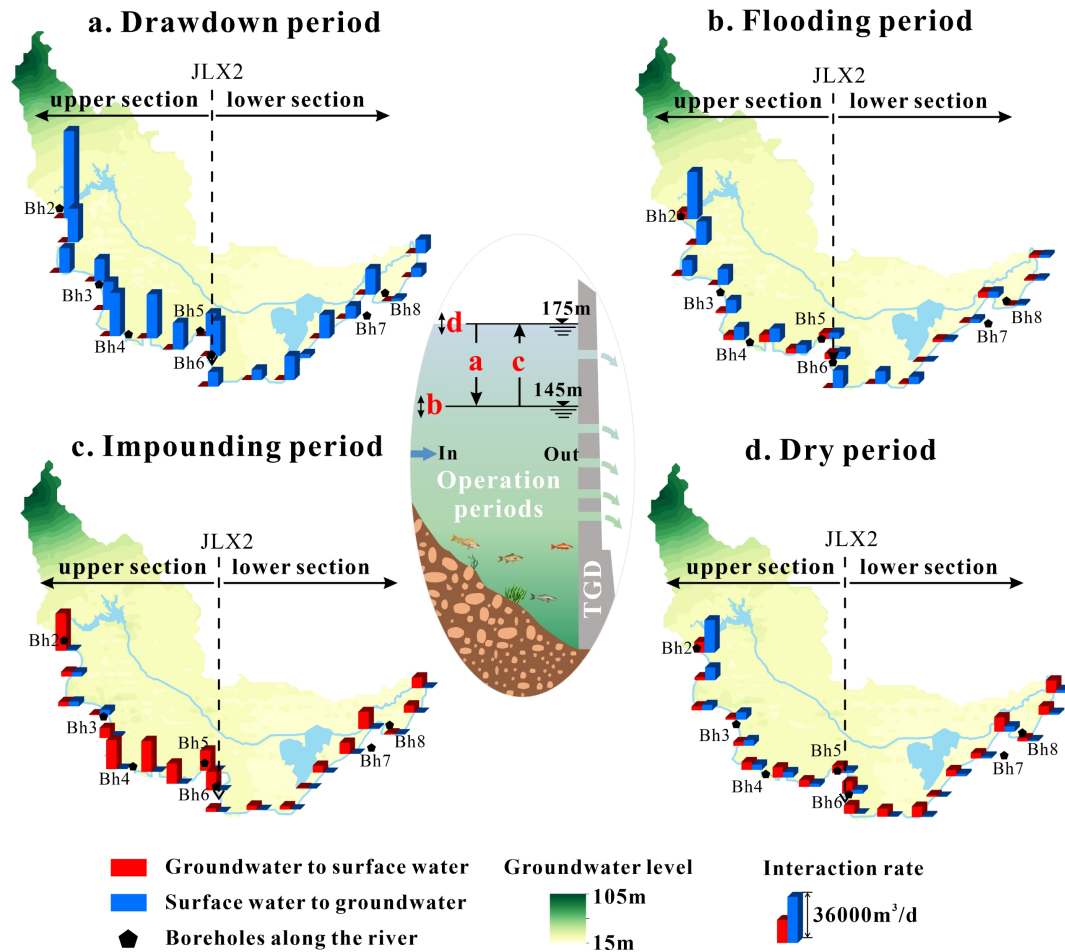


406
 407 Figure 5: Fitting between the observed groundwater levels and the calculated ones at six monitoring
 408 wells during the simulated period.

409 **4.3 Yangtze River-groundwater interaction under TGD regulation:**
 410 **Spatiotemporal patterns**

411 Figure 6 illustrates the daily exchange volume between the Yangtze River and
 412 groundwater in the mainstream within the Four-Lake Basin, calculated by the SWAT-
 413 MODFLOW model at 15-km intervals. The relative magnitudes are represented by
 414 bar charts, with blue and red indicating groundwater recharge from and discharge to
 415 the Yangtze River, respectively. The four subplots correspond to the four scheduling

416 periods of the TGD: a. Drawdown period. This period refers to the pre-flood water
417 release phase, during which the water level of the TGD is lowered below the flood
418 limit level through controlled discharge to prepare for flood peak retention and
419 attenuation; b. Flooding period. This period represents the subsequent flood season,
420 during which the reservoir intercepts floods and adjusts the timing of downstream
421 flood peaks; c. Impounding period. This period denotes the post-flood water storage
422 phase, where water at the end of the flood season is stored for use during dry periods;
423 d. Dry period. This period is set for the water stored in the previous period to release
424 to supplement downstream flow during dry seasons. The results in the figure represent
425 the daily average exchange rate over all days within each operational period.



426

427 Figure 6: Spatial variations in interaction rates (average of 2011 and 2013, m³/d) between the Yangtze
 428 River and groundwater in the Four-Lake Basin during the four operational periods of the TGD. Red
 429 histograms denote groundwater discharge to surface water; blue histograms denote surface-water
 430 recharge to groundwater. TGD operational periods: a. Drawdown period, b. Flooding period, c.
 431 Impounding period and d. Dry period. The vertical dashed line indicates a spatial demarcation for
 432 different interaction patterns along the river reach.

433 As shown in Fig. 6, river-to-aquifer recharge dominates during both the
 434 drawdown period and the flooding period, while aquifer-to-river discharge prevails in
 435 the other two periods. Moreover, the recharge rate during the drawdown period is
 436 significantly higher than that during the flooding period. It occurs because during the

437 drawdown period, the TGD gradually lowers the reservoir level from 175 m at the end
438 of the previous winter to below 145 m (referenced to the Yellow Sea Datum) and
439 releases the incoming spring flows upstream. The substantial outflow leads to a
440 marked rise in the downstream river stage, amplifying the hydraulic gradient between
441 the river and adjacent groundwater and driving strong river-to-aquifer recharge.
442 During the flooding period, groundwater levels are considerably elevated due to
443 rainfall infiltration and surface water recharge in the Four-Lake basin, which have
444 been confirmed by our SWAT-MODFLOW simulation. Additionally, TGD
445 operations during this period aim to attenuate downstream flood peaks for safety,
446 thereby significantly reducing the hydraulic gradient between the river and
447 groundwater compared to that during the drawdown period. It explains why the
448 apparent river-groundwater exchange is weaker during the hydrologically more
449 dynamic flooding period, as observed in Fig. 6b.

450 The intensity of aquifer-to-river discharge is higher during the impounding
451 period than during the dry period. This difference arises because during the
452 impounding period, groundwater levels remain elevated following the end of the
453 flood season, while the TGD begins to impound upstream water in preparation for the
454 dry-season water supply. This process enlarges the hydraulic gradient between
455 groundwater and the Yangtze River. In contrast, during the dry period, groundwater
456 levels have declined, and the TGD releases water to supplement downstream flow,
457 which reduces the hydraulic gradient between groundwater and the river. It explains
458 why the aquifer-to-river discharge intensity is stronger during the impounding period
459 than during the dry period.

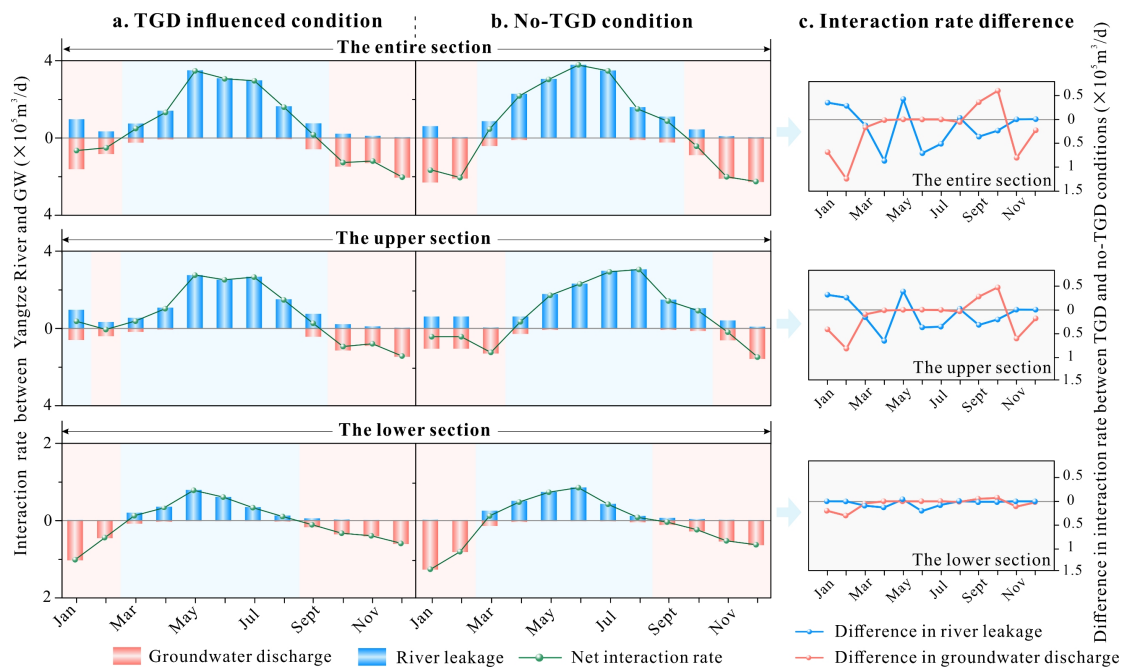
460 In addition, dividing the Yangtze River at the profile JLX2 into an upper section
461 and a lower section (as shown in Fig. 6) reveals consistently higher exchange rates in
462 the upper one. This pattern arises because the upper section is closer to and more

463 influenced by TGD regulation than the lower section, leading to larger stage
464 fluctuations and weaker along-stream attenuation, which together enhance the
465 hydraulic gradient. In contrast, the lower section, characterized by a wider channel
466 and greater hydraulic connectivity with tributaries, exhibit a comparatively weaker
467 response to the Three Gorges Dam operations. As shown in Fig. A5 in the Appendix
468 A, wavelet coherence analysis reveals that with increasing distance from the TGD, the
469 downstream river stage exhibits a progressive damping in its response to reservoir
470 release variations, accompanied by a lengthening phase lag (see Appendix A).
471 Moreover, the along-river lithology profile in Fig. 3b reveals a distinct shift in aquifer
472 composition: the upstream banks are dominated by highly permeable gravel and
473 coarse sand, which sharply contrasts with the less permeable fine sand that constitutes
474 the downstream deposits. The strong heterogeneity of the riparian stratigraphy is also
475 a significant factor contributing to the weaker downstream interactive strength
476 compared to that upstream. Notably, the spatial contrast in exchange intensity
477 revealed by the SWAT-MODFLOW simulations is consistent with the lateral
478 influence patterns identified in Section 4.1, indicating that along-river geological
479 heterogeneity and Yangtze River stage variability jointly control the interaction
480 between lateral groundwater and the Yangtze River.

481 **4.4 Yangtze River-groundwater interaction with and without TGD: A** 482 **counterfactual comparison**

483 Against the backdrop of numerous factors influencing Yangtze River-
484 groundwater interactions, this study isolated the effect of TGD regulation by
485 implementing simulated "no-TGD" river stages from Wang et al. (2013) in the
486 SWAT-MODFLOW model. All other input data, such as precipitation, evaporation,
487 groundwater levels, and tributary/lake stages, remained unchanged. This setup

488 produced the results of river leakage to groundwater and groundwater discharge to
 489 river shown in Figs. 7(a) and 7(b), respectively: they illustrate the monthly variations
 490 in daily exchange rates between the Yangtze River and groundwater for the upper
 491 section, lower section, and the entire mainstream of the Four-Lake basin, demarcated
 492 by the Profile JLX2. Here, the daily interaction rate represents the monthly total
 493 interaction amount averaged over all the days in that month, visualized using bar
 494 charts: red bars indicate aquifer-to-river discharge, and blue bars represent river-to-
 495 aquifer recharge. The green line graph in Figs. 7(a) and 7(b) depict the net daily
 496 exchange, calculated as river leakage minus groundwater discharge. Fig. 7(a) shows
 497 simulation results influenced by TGD operation (corresponding to those in Fig. 6),
 498 while Fig. 7(b) presents those without TGD. By subtracting the daily interaction rates
 499 in Fig. 7(b) from those in Fig. 7(a), we obtain the differences in these rates between
 500 the scenarios with and without the TGD, as shown in Fig. 7(c).



501

502 Figure 7: Temporal variations in the river leakage rates, groundwater discharge rates and net exchange
503 rates between the Yangtze River and groundwater under a. TGD-influenced and b. no-TGD conditions.
504 Fluxes are positive for river leakage to the aquifer and negative for groundwater discharge to the river.
505 c. Figure of interaction rate difference between TGD and no-TGD conditions in river leakage and
506 groundwater discharge. More detailed information can be found in Table A3.

507 Figure 7(b) shows that regardless of TGD operation, the Yangtze Rive leakage to
508 groundwater dominates from March to September in both the upper and lower
509 sections of the Four-Lake basin. In contrast, groundwater discharge to the Yangtze
510 River prevails from October to February of the following year. Across the entire
511 section of stream, the peak net exchange rate occurs in June, reaching 3.77×10^5 m³/d.
512 Spatially, the net flow direction (river leakage versus groundwater discharge) differs
513 between the upper and lower sections. In the upper section, the rate of river leakage to
514 groundwater consistently exceeds the discharge rate, regardless of TGD regulation.

515 With a comparison between Figs. 7(a) and 7(b) by calculating the average net
516 exchange rates for both flooding season (from June to September) and dry period
517 (from November to April), one can find that TGD operations significantly suppress
518 the natural river-groundwater exchange. Under TGD regulation, the net exchange rate
519 across the entire section decreased by 19.3% and 41.8% during the flooding and dry
520 periods, respectively, compared to natural conditions. This suppression was more
521 pronounced in the upper section, where the net exchange dropped by 40.6% during
522 the dry period, contrasting with a decrease of 23.8% in the lower section. In addition,
523 it can be visually inferred from Fig. 7(c) that a considerable number of values lie
524 below zero. This indicates that, compared to the natural conditions, TGD operations
525 lead to a reduction in river leakage to groundwater for nine months of the year and a
526 decrease in groundwater discharge to the river for ten months in the upper section.
527 Notably, in the lower section, the fluxes in both directions (river leakage and
528 groundwater discharge) are reduced throughout nearly the entire year.

529 These findings demonstrate that the TGD attenuates flood peaks and elevates
530 low flows, thereby reducing the seasonal amplitude of river stages and narrowing the
531 river-aquifer hydraulic gradient. Consequently, the exchange dynamics become more
532 balanced and stable. The upper section, being directly subject to regulatory releases,
533 exhibits a more pronounced response in net exchange, particularly during the dry
534 season. As also evident from the mapped zone of the Yangtze River's lateral influence
535 on groundwater in Fig. 3, the groundwater response to river stage changes is visibly
536 weaker in the lower section, particularly near Honghu Lake, compared to the upper
537 section. As shown by the net interaction curve for the upper section (Fig. 7), the
538 period from January to March, which was naturally characterized by groundwater
539 discharge to the river, transitions to a state of weak river leakage to the aquifer
540 following the TGD-induced rise in dry-season river stage. This flow reversal occurs
541 because the dry-season hydraulic gradient is inherently small; thus, even a modest
542 stage increase can induce a substantial relative change, making the regulatory
543 influence more pronounced during dry months than in the flood season.

544 **5 Limitations and Future Work**

545 This study has its potential sources of uncertainty, which arises from the spatial
546 sparsity of observation well data used for model calibration and the inability of the
547 one-way coupled model to simulate groundwater discharge to surface water. Besides,
548 several limitations should be acknowledged: Firstly, the lateral influence distance of
549 the Yangtze River was analyzed using the full-year observed amplitude of both river
550 stage and groundwater level fluctuations, making it difficult to interpret how this
551 result varies across different seasons or hydrological year types. Therefore, a more
552 detailed characterization of intra-annual variability would require longer monitoring

553 records with higher temporal resolution, which will be addressed in future work.
554 Secondly, in such a riparian wetland environment, the sources of groundwater
555 recharge along the riverbank has not been analyzed in detail. Future studies will
556 therefore consider tracer-based investigations to further evaluate groundwater sources
557 associated with major lakes, rivers, wetlands, and localized upland areas in the Four-
558 Lake Basin. Thirdly, regarding the spatial influence of the Yangtze River on lateral
559 groundwater, providing a calculation result without the TGD, similar to the numerical
560 modeling approach, would greatly help deepen the discussion on this topic. However,
561 the scarcity of observed groundwater data prior to the construction of the TGD has
562 constrained the successful implementation of this idea.

563 **6 Conclusion**

564 This study integrated large-scale monitoring data from multiple profiles along
565 the Yangtze River in the Four-Lake Basin, on which a spatial response analysis of
566 water levels was performed followed by a coupled surface water-groundwater
567 modeling framework. Then, the interactions between the Yangtze River and
568 groundwater were systematically investigated through both qualitative and
569 quantitative analyses. The key findings are as follows:

570 (1) Spatial variability of the Yangtze River influence. The lateral influence zone
571 of the Yangtze River on groundwater in the Four-Lake Basin has been quantified for
572 the first time, revealing a band-like pattern with a high degree of spatial heterogeneity.
573 The lateral influence range varies from 1.94 km (HH1 profile) to 12.77 km (ZJ profile)
574 across the Four-Lake Basin.

575 (2) Performance of the newly proposed model. Given the significant influence of
576 rainfall and the surface water network on groundwater in the Four-Lake basin, the

577 SWAT-MODFLOW model is capable of accurately quantifying the exchange fluxes
578 between the Yangtze River and groundwater.

579 (3) Spatial-temporal interaction dynamics between the Yangtze River and
580 groundwater. Temporally, the Yangtze River leakage to groundwater is greater during
581 the drawdown period than during the flooding period. Conversely, groundwater
582 discharge to the Yangtze river is higher in the impounding period than in the dry
583 period. This dynamic is dictated by the combined effects of seasonal TGD regulation
584 and the local hydroclimate. Spatially, the interaction intensity between the Yangtze
585 River and groundwater is markedly higher in the upper section of the Four-Lake
586 Basin than the lower section, which is attributed to the integrated influences of the
587 TGD, the thalweg configuration, and riparian hydrogeology.

588 (4) The impacts of the TGD operation on the Yangtze River-groundwater
589 interaction. By modulating river stages, TGD operations reduce temporal variability
590 in Yangtze River-groundwater exchange rates, thereby promoting more balanced and
591 stable dynamics. This effect is most direct and pronounced in the upper section during
592 the dry period, whereas its influence attenuates downstream.

593

594

595 **Appendix A**

596

597

Table A1 Aquifer hydrogeologic parameters for MODFLOW model.

Parameter Zone	Horizontal Conductivity		Vertical Conductivity		Specific Yield	Specific Storage
	K_x and K_y (m/d)		K_z (m/d)		S_y	S_s (L^{-1})
	Unconfined Aquifer	Confined Aquifer	Unconfined Aquifer	Confined Aquifer	Unconfined Aquifer	Confined Aquifer
1	1.00	9.75	0.150	1.1		0.0004
2	1.5	16	0.302	1.6	0.021	0.0022
3	0.79	7.7	0.120	0.85		0.001
4	0.54	4.9	0.081	0.57		0.0023

598

599

600

Table A2 SWAT model calibrated parameters with adjusted values and sensitivity ranking.

Symbol	scale	Calibrated Value	<i>t</i> -value	<i>p</i> -value	Sensibility
GWQMN	0-5000	186.90	-30.89	0.00	1
REVAPMN	0-500	188.31	15.60	0.00	2
GW_DELAY	0-500	232.39	-1.97	0.05	3
CH_N2	-0.01-0.3	0.11	1.91	0.06	4
SOL_BD	0.9-2.5	1.13	1.79	0.07	5
CH_N1	0.01-30	20.30	-1.48	0.14	6
CH_K2	-0.01-500	27.39	-1.22	0.22	7
SURLAG	0.05-24	15.11	-1.21	0.23	8
GW_REVAP	0.02-0.2	0.17	-1.20	0.23	9
SOL_AWC	0-1	0.00	0.90	0.37	10
ESCO	0.01-1	0.36	0.88	0.38	11
OV_N	0.01-30	17.89	-0.81	0.42	12
ALPHA_BNK	0-1	0.33	-0.79	0.43	13
ALPHA_BF	0-1	0.22	-0.47	0.64	14
SOL_K	0-2000	1766.62	0.38	0.70	15
EPCO	0.01-1	0.38	0.16	0.87	16
CN2	35-98	35.34	-0.01	0.99	17

601

602 Table A3 Average river leakage, groundwater discharge, and net exchange rates (average of 2011 to
603 2013) under TGD regulated operation and natural conditions between the Yangtze River and
604 groundwater for the entire section, upper section, and lower section.

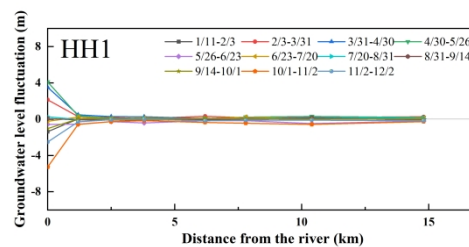
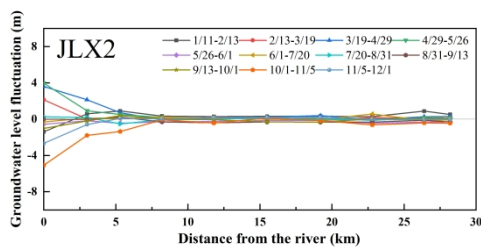
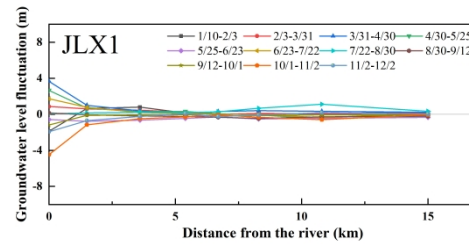
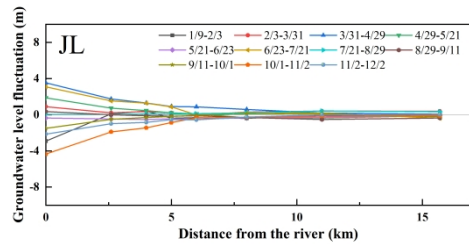
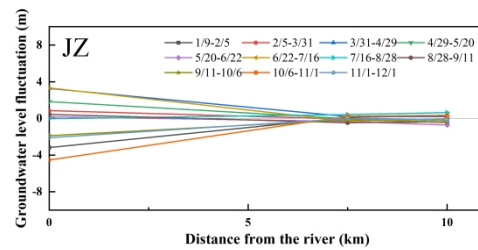
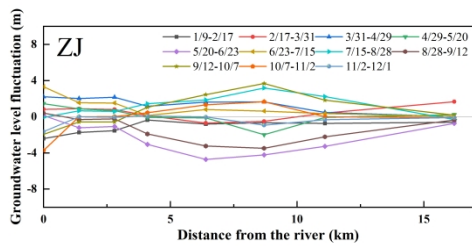
Month	TGD regulated operation (m ³ /d)			Natural condition (m ³ /d)		
	GW to SW interaction rate	SW to GW interaction rate	Net interaction rate	GW to SW interaction rate	SW to GW interaction rate	Net interaction rate
The entire section						
January	160398.61	95125.29	-65273.32	228615.16	60134.45	-168480.71
February	82495.96	31721.82	-50774.14	207866.07	3207.19	-204658.88
March	23711.71	72382.68	48670.97	39499.77	85539.23	46039.45
April	6623.12	138788.77	132165.65	8323.54	226616.07	218292.53
May	243.95	346652.48	346408.53	392.89	303461.94	303069.04
June	164.13	306211.00	306046.87	177.75	376947.00	376769.25
July	820.53	296601.61	295781.08	738.01	347322.58	346584.57
August	3511.69	161664.84	158153.15	8772.14	158542.26	149770.11
September	57918.17	73367.00	15448.83	21667.64	109546.30	87878.66
October	147234.71	19725.15	-127509.56	86604.52	43101.06	-43503.45
November	128486.87	8695.77	-119791.10	208785.13	8053.23	-200731.90
December	204551.52	1709.64	-202841.88	227181.03	1014.45	-226166.58
The upper section						
January	58348.03	95037.48	36689.45	102956.55	60063.03	-42893.52
February	38014.14	31633.79	-6380.36	127649.18	3134.64	-124514.54
March	16301.00	53726.03	37425.03	26561.48	60730.62	34169.13
April	4151.07	106185.73	102034.66	5809.77	176407.07	170597.30
May	119.41	273851.55	273732.14	193.20	229956.61	229763.42
June	0.00	251251.33	251251.33	43.90	291955.00	291911.10
July	189.88	265419.35	265229.48	195.26	304419.35	304224.09
August	1747.66	149041.61	147293.95	5534.11	146825.81	141291.70
September	41711.41	67952.03	26240.62	11612.61	103078.03	91465.43
October	112226.70	17772.32	-94454.38	59672.18	39762.87	-19909.31
November	88397.23	8008.71	-80388.52	155803.43	7426.35	-148377.08
December	144907.90	1609.14	-143298.76	164598.90	935.00	-163663.90
The lower section						
January	102049.81	88.41	-101961.40	125658.55	71.12	-125587.42
February	44481.75	88.01	-44393.74	80217.18	72.57	-80144.61

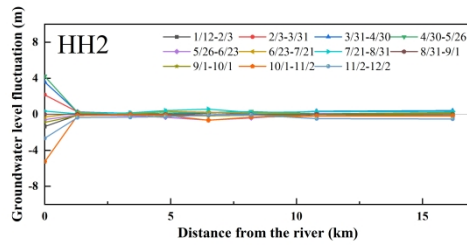
March	7410.79	19464.46	12053.67	12938.26	24809.01	11870.76
April	2472.04	34925.19	32453.15	2513.73	50209.80	47696.07
May	124.54	78462.61	78338.07	199.69	73506.32	73306.63
June	164.13	60520.87	60356.74	133.85	84992.97	84859.12
July	630.65	34033.13	33402.48	542.75	42902.87	42360.12
August	1764.04	12076.83	10312.79	3238.03	11716.11	8478.07
September	16207.16	4955.09	-11252.07	10055.03	6469.54	-3585.49
October	35008.08	1889.88	-33118.21	26932.46	3337.93	-23594.54
November	40089.60	684.73	-39404.87	52981.83	626.87	-52354.95
December	59643.16	100.48	-59542.68	62582.29	79.45	-62502.84

605

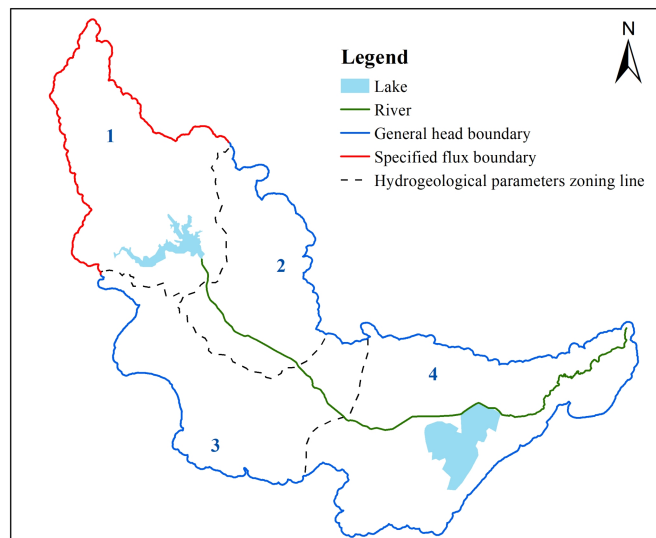
606

607

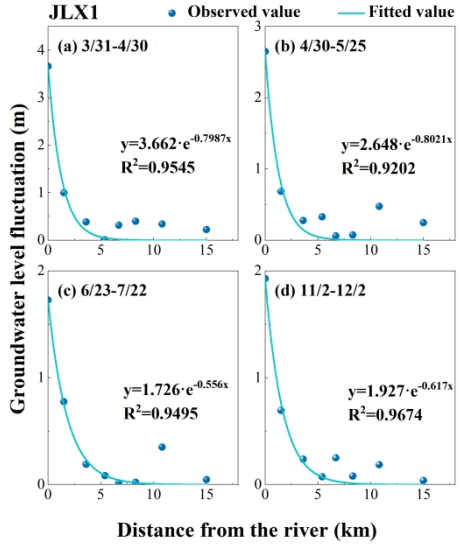
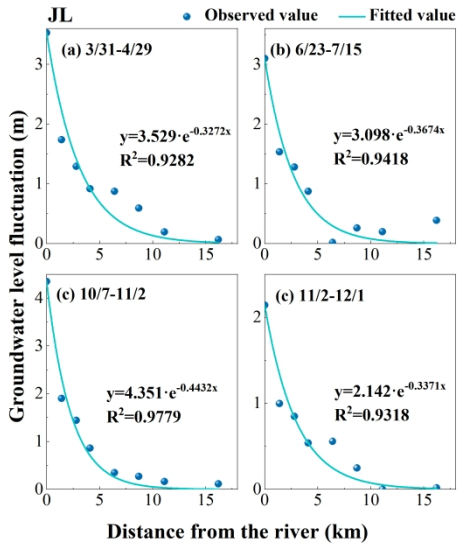
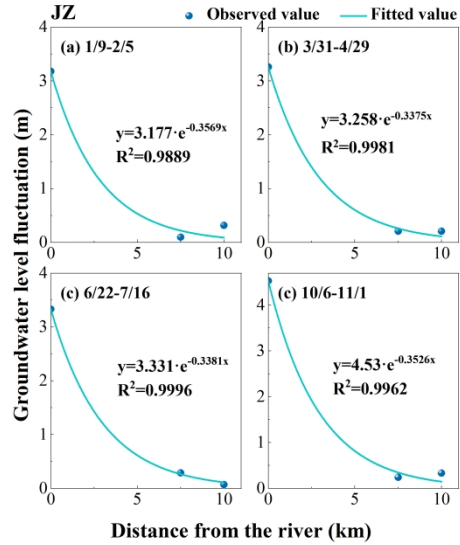
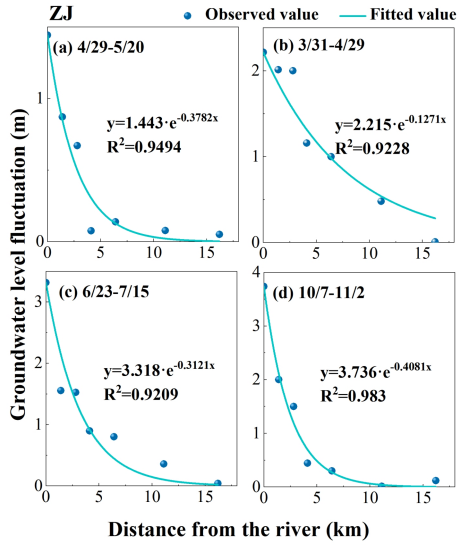


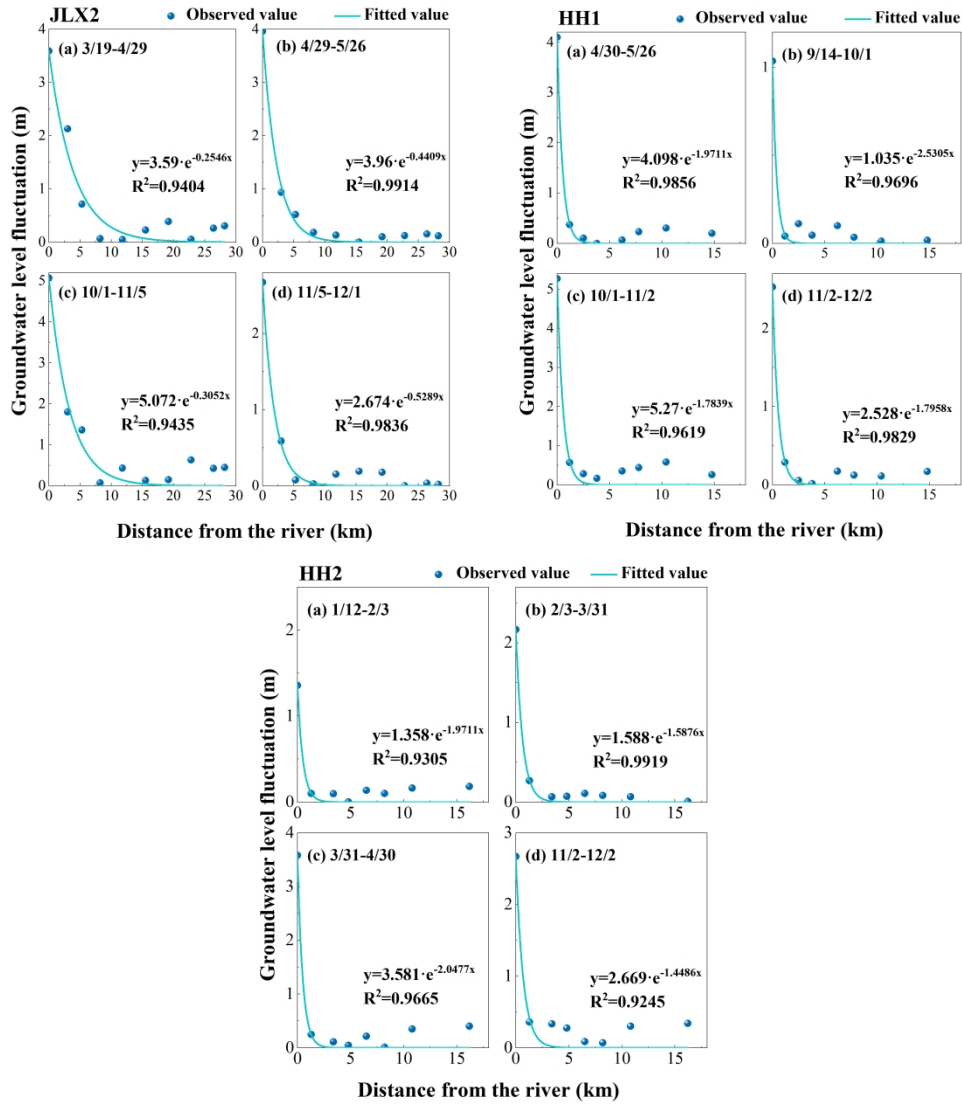


608 Figure A1. Groundwater level fluctuation y versus distance from the river x for each monitoring profile.
 609 In the legend, the A and B in "A/B" represent month and data, respectively
 610

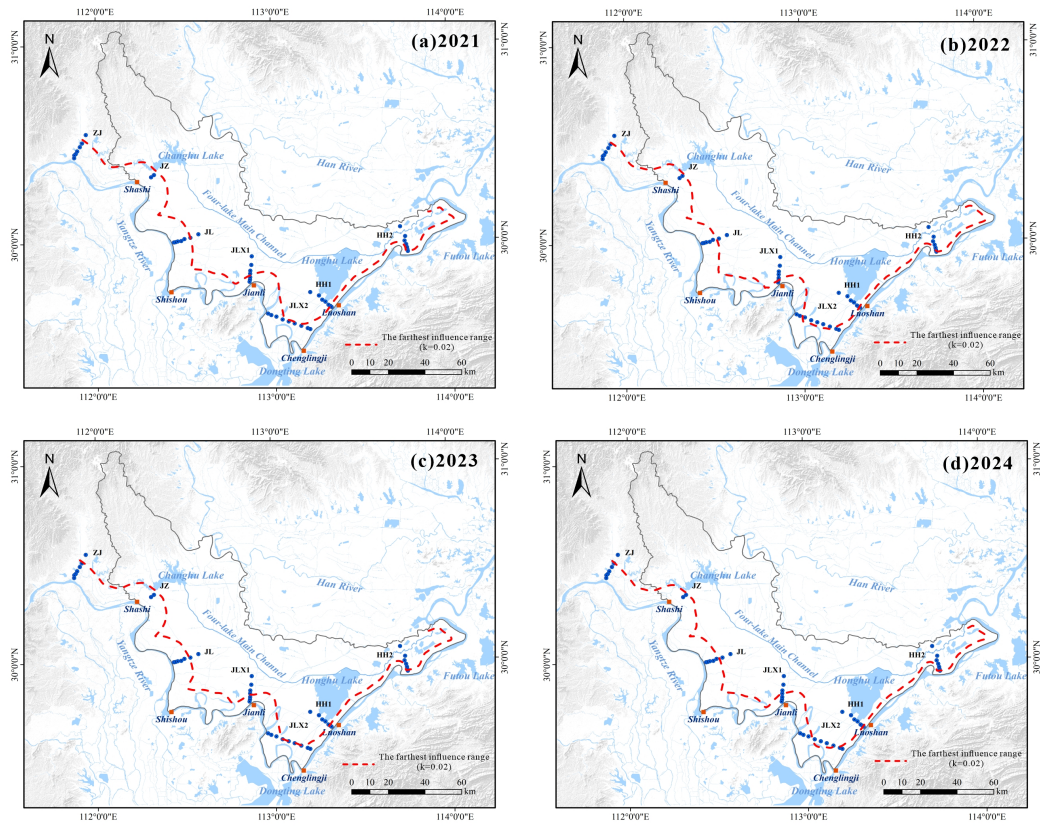


611
 612 Figure A2. Groundwater model boundary and hydrogeologic parameter zones.





613 Figure A3. The Fitting curves of groundwater level fluctuation versus distance from the river for each
 614 monitoring profile.
 615



616

617 Figure A4. The spatial distribution of influence range of Yangtze River in four different years

618

619 **Wavelet coherence analysis of reservoir release and downstream river stage**

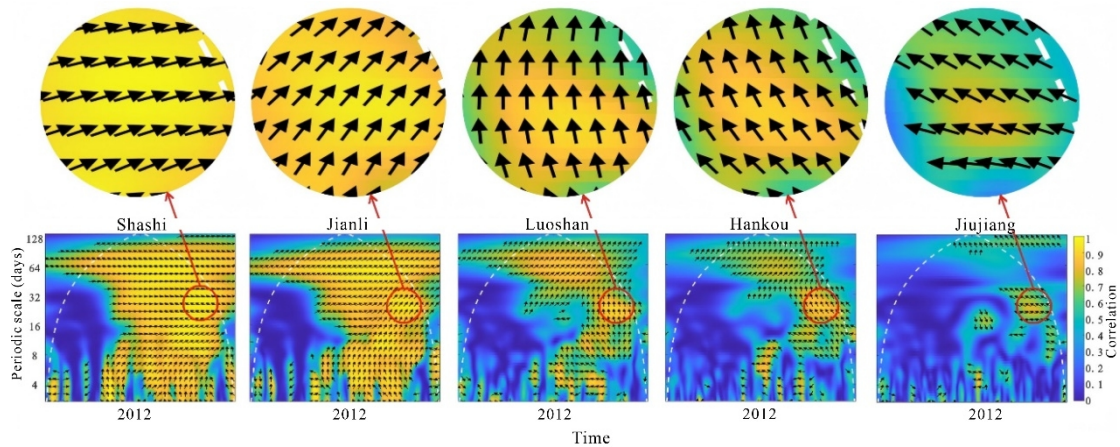
620

621 Figure A5 is adapted from a previous study by the authors, in which continuous
 622 wavelet transform (CWT; Torrence et al., 1997) was applied to analyze the time-
 623 frequency relationship between discharge from the Three Gorges Reservoir and daily
 624 water levels at five hydrological stations along the middle Yangtze River (Shashi,
 625 Jianli, Luoshan, Hankou, and Jiujiang). The figure presents results for the year 2012
 626 as a representative example.

626

627 In the wavelet coherence spectra, warm colors indicate high coherence and cool
 628 colors indicate low coherence. A downstream decrease in high-coherence regions is

628 evident among the five stations, with the most pronounced attenuation occurring at
629 Luoshan, suggesting a weakening influence of reservoir regulation with increasing
630 distance and tributary inflow (notably from Dongting Lake). The arrows denote phase
631 relationships between the two sets of time series data, showing a progressive increase
632 in phase lag from upstream to downstream, which indicates delayed river-stage
633 responses to reservoir discharge variations.



634 Figure A5. Wavelet correlation between the Three Gorges Reservoir water level and the water
635 levels at Shashi, Jianli, Luoshan, Hankou, and Jiujiang hydrological stations on the Yangtze River
636 in 2012.
637
638

639 Code and data availability

640 Additional information regarding methodology and results is provided in the
641 Supplement.

642 Author contributions

643 Qi Zhu: conceptualization, formal analysis and writing; Ye Kang: methodology,
644 investigation and drawing; Zhang Wen: project administration and software; Hui Liu:

645 Funding acquisition and idea; Luguang Liu: monitoring work; Yan Li: field data
646 collection; Xu Li: model support, Eungyu Park: supervision and validation.

647 **Competing interests**

648 The authors declare that they have no conflict of interest.

649 **Acknowledgements**

650 We would like to appreciate the constructive comments of the handling editor
651 and three anonymous reviewers, who help us improve the quality of the paper. It is
652 worth mentioning that the handling editor has put great effort into carefully
653 examining the figures, tables, punctuation, and typos in the manuscript. We sincerely
654 admire the handling editor's diligent and responsible attitude.

655 **Financial support**

656 This research was partially supported by the National Natural Science
657 Foundation of China (Grant Numbers: U2340206; U23A2042; 42572313; 42272290)
658 the Natural Science Foundation of Hubei Province (2023AFD194), and the Hubei
659 Province Science and Technology Innovation Platform Project (Grant Number
660 2025CSA007).

661 **References**

662 Aliyari, F., Bailey, R. T., Tasdighi, A., Dozier, A., Arabi, M., Zeiler, K.: Coupled
663 SWAT-MODFLOW model for large-scale mixed agro-urban river basins,

664 Environ. Modell. Softw., 115, 200–210, doi: 10.1016/j.envsoft.2019.02.014,
665 2019.

666 Deng, K., Yang, S., Lian, E., Li, C., Yang, C., Wei, H.: Three Gorges Dam alters the
667 Changjiang (Yangtze) river water cycle in the dry seasons: Evidence from H-O
668 isotopes, *Sci. Total Environ.*, 562, 89–97, doi: 10.1016/j.scitotenv.2016.03.213,
669 2016.

670 Dewey, C., Fox, P. M., Bouskill, N. J., Dwivedi, D., Nico, P., Fendorf S.: Beaver
671 dams overshadow climate extremes in controlling riparian hydrology and water
672 quality. *Nat. Commun.*, 13, 6509, doi: 10.1038/s41467-022-34022-0, 2022.

673 Du, Y., Ma, T., Deng, Y., Shen, S., Lu, Z.: Characterizing groundwater/surface-water
674 interactions in the interior of Jiangnan Plain, central China, *Hydrogeol. J.*, 26(4),
675 1047–1059, doi: 10.1007/s10040-017-1709-7, 2018.

676 Esri.: World Ocean Base [Data set]. ArcGIS Online. Retrieved from
677 https://services.arcgisonline.com/ArcGIS/rest/services/Ocean/World_Ocean_Base/MapServer, 2023.
678

679 Gao, Y., Zhang, W., Li, Y., Wu, H., Yang, N., Hui, C.: Dams shift microbial
680 community assembly and imprint nitrogen transformation along the Yangtze
681 River, *Water Res.*, 189, 116579, doi:10.1016/j.watres.2020.116579, 2021.

682 Guo, W., Zhou, H., Jiao, X., Huang, L., Wang, H.: Evaluation of hydrological regime
683 alteration and ecological effects in the middle and lower of the Yangtze River,
684 China, *Water Supply*, 22(6), 5957-5973., doi: 10.2166/ws.2022.229, 2022.

685 He B., Cai S.: The Three-Gorge Project and dynamics of shallow confined water in
686 the area of the middle reaches of the Yangtze River. *Resources and Environment*
687 *in the Yangtze Basin*, 8(1), doi: CNKI:SUN:CJLY.0.1999-01-014, 1999.

688 Hu, M., Yao, M., Wang, Y., Pan, Z., Wu, K., Jiao, X., Chen, D.: Influence of nitrogen
689 inputs, dam construction and landscape patterns on riverine nitrogen exports in

690 the Yangtze River basin during 1980–2015, *J. Hydrol.*, 617, 129109, doi:
691 10.1016/j.jhydrol.2023.129109, 2023.

692 Hu, M., Zhou, P., Chen, C.: Study on coupling of typical elements in surface water
693 and groundwater in the middle reaches of the Yangtze River, China, *J. Hydrol.*,
694 626, 130298, doi: 10.1016/j.jhydrol.2023.130298, 2023.

695 Huang, P., Zhou, A., Ma, C., Guo, J., Wang, Y., Fan, W., Li, W.: Impact of the Three
696 Gorges Dam on the spatial and temporal variation of groundwater level in
697 Jiangnan Plain using STL algorithm, *Environ. Earth Sci.*, 82(18), 417, doi:
698 10.1007/s12665-023-11110-y, 2023.

699 Huang, S., Xia, J., Zeng, S. Wang, Y., She, D.: Effect of Three Gorges Dam on
700 Poyang Lake water level at daily scale based on machine learning, *Journal of*
701 *Geographical Sciences*, 31, 1598-1614, doi: 10.1007/s11442-021-1913-1, 2021.

702 Jiang, X., Ma, R., Ma, T., Sun, Z.: Modeling the effects of water diversion projects on
703 surface water and groundwater interactions in the central Yangtze River basin,
704 *Sci. Total Environ.*, 830, 154606, doi: 10.1016/j.scitotenv.2022.154606, 2022.

705 Khaleghi, M.R., Hosseini, S.H.: Using SWAT and SWAT-CUP for hydrological
706 simulation and uncertainty analysis of the arid and semiarid watersheds (Case
707 study: Zoshk Watershed, Shandiz, Iran). *Appl. Water Sci.*, 14, 266,
708 doi:10.1007/s13201-024-02327-8, 2024

709 Lai, X., Zou, H., Jiang, J., Jia, J., Liu, Y., Wei, W.: Hydrological dynamics of the
710 Yangtze River-Dongting lake system after the construction of the three Gorges
711 dam, *Scientific Reports*, 15(1), 50, doi: 10.1038/s41598-024-83751-3, 2025.

712 Lan, Y., He, Y., Yu, Q., Song, Q.: Delineating sources of groundwater recharge in an
713 arsenic-affected aquifer in Jiangnan Plain using stable isotopes, *Hydrological*
714 *Processes*, 39, e70050, doi: 10.1002/hyp.70050, 2025.

715 Li, Y., Jing, G., Aiming, C., Jie, G., Yilin, W., Yao, Y., Youping, Z., Bo, Y.:
716 Characteristics of groundwater in the cold waterlogged paddy field of the
717 Jiangnan Plain, *Resources Environment & Engineering*, 37, 163, doi:
718 10.16536/j.cnki.issn.1671-1211.2023.02.005, 2023.

719 Liu, Y., Wang, H., Wu, Y., Zhao, Y., Ren, X.: Aquifer response to stream-stage
720 fluctuations: field tests and analytical solution for a case study of the Yangtze
721 River in Wuhan, China, *Water*, 13(17), 2388, doi: 10.3390/w13172388, 2021.

722 Maavara, T., Chen, Q., Van Meter, K., Brown, L. E., Zhang, J., Ni, J., Zarfl, C.: River
723 dam impacts on biogeochemical cycling. *Nat. Rev. Earth Env.*, 1(2), 103-116,
724 doi:10.1038/s43017-019-0019-0, 2020

725 Palmer, M., Ruhi, A.: Linkages between flow regime, biota, and ecosystem processes:
726 Implications for river restoration, *Science*, 365, 1264, doi:
727 10.1126/science.aaw2087, 2019.

728 Poff, N. L., Allan, J. D., Bain, M. B., Karr, J. R., Prestegard, K. L., Richter, B. D.,
729 Sparks, R. E., Stromberg, J. C.: The natural flow regime, *Bioscience*, 47(11),
730 769-784, doi: 10.2307/1313099, 1997.

731 Pulido-Velazquez, M., Peña-Haro, S., García-Prats, A., Mocholi-Almudever, A. F.,
732 Henriquez-Dole, L., Macian-Sorribes, H., Lopez-Nicolas, A.: Integrated
733 assessment of the impact of climate and land use changes on groundwater
734 quantity and quality in the Mancha Oriental system (Spain), *Hydrol. Earth Syst.*
735 *Sci.*, 19, 1677–1693, doi: 10.5194/hess-19-1677-2015.

736 Song, X., Chen, X., Zachara, J. M., Gomez-velez, J. D., Shuai, P., Ren, H., Hammond,
737 G. E.: dynamics control transit time distributions and biogeochemical reactions
738 in a dam-regulated river corridor, *Water Resour. Res.*, 56(9), e2019WR026470,
739 doi: 10.1029/2019WR026470.

- 740 Sun, Z., Huang, Q., Opp, C., Hennig, T., Marold, U.: Impacts and implications of
741 major changes caused by the Three Gorges Dam in the middle reaches of the
742 Yangtze River, China, *Water Resour. Manag.*, 26, 3367-3378, doi:
743 10.1007/s11269-012-0076-3, 2012.
- 744 Torrence C, Compo G P.: A Practical Guide to Wavelet Analysis, *Bulletin of the*
745 *American Meteorological Society*, 79(1), 61, 1997, doi: 10.1175/1520-
746 0477(1998)079<0061:apgtwa>2.0.co;2
- 747 Van Cappellen, P., Maavara, T.: Rivers in the Anthropocene: Global scale
748 modifications of riverine nutrient fluxes by damming, *Ecohydrol. Hydrobiol.*,
749 16(2), 106-111, doi: 10.1016/j.ecohyd.2016.04.001, 2016.
- 750 Wang, J., Sheng, Y., Gleason, C.J., Wada, Y.: Downstream Yangtze River levels
751 impacted by Three Gorges Dam, *Environ. Res. Lett.*, 8(4), 044012, doi:
752 10.1088/1748-9326/8/4/044012, 2013.
- 753 Wang, J., Wörman, A.: Spectral analysis of river resistance and aquifer diffusivity in
754 a river-confined aquifer system. *Water Resour. Res.*, 55(10), 8046–8060, doi:
755 10.1029/2018WR024639, 2019.
- 756 Wang, Y., Rhoads, B. L., Wang, D.. Assessment of the flow regime alterations in the
757 middle reach of the Yangtze River associated with dam construction: potential
758 ecological implications, *Hydrol. Processes*, 30(21), 3949-3966, doi:
759 10.1002/hyp.10921, 2016.
- 760 Wen, Z., Zhan, H., Wang, Q., Liang, X., Ma, T., Chen, C.: Well hydraulics in
761 pumping tests with exponentially decayed rates of abstraction in confined
762 aquifers, *J. Hydrol.*, 548, 40-45, doi: 10.1016/j.jhydrol.2017.02.046, 2017.
- 763 World Bank, 2023. Yangtze River Protection and Ecological Restoration Program
764 Program for Results (Hubei).

765 Wu, X., Wang, L., Cao, Q., Niu, Z., Dai, X.: Regional climate change and possible
766 causes over the Three Gorges Reservoir Area, *Sci. Total Environ.*, 903, 166263,
767 doi: 10.1016/j.scitotenv.2023.166263, 2023.

768 Xie, Y., Tang, Y., Chen, X., Li, F., Deng, Z.: The impact of Three Gorges Dam on the
769 downstream eco-hydrological environment and vegetation distribution of East
770 Dongting Lake, *Ecohydrology*, 8(4), 738-746, doi: 10.1002/eco.1543, 2014.

771 Xiong, J., Yin, J., Kyaw Tha Paw U, Zhao, S., Qiu, G., Liu, Z.: How the three Gorges
772 Dam affects the hydrological cycle in the mid-lower Yangtze River: a
773 perspective based on decadal water temperature changes, *Environ. Res. Lett.*, 15,
774 014002, doi: 10.1088/1748-9326/ab5d9a, 2020.

775 Yang, Y., Yuan, Y., Xiong, G., Yin, Z., Guo, Y., Song, J., Zhu, X., Wu, J., Wang, J.,
776 Wu, J.: Patterns of nitrate load variability under surface water-groundwater
777 interactions in agriculturally intensive valley watersheds, *Water Res.*, 267,
778 122474, doi: 10.1016/j.watres.2024.122474, 2024.

779 Yang, S., Milliman, J. D., Xu, K., Deng, B., Zhang, X., Luo, X.: Downstream
780 sedimentary and geomorphic impacts of the Three Gorges Dam on the Yangtze
781 River, *Earth-Sci. Rev.*, 138, 469-486, doi: 10.1016/j.earscirev.2014.07.006, 2014.

782 Yang, S., Zhang, J., Xu, X.: Influence of the Three Gorges Dam on downstream
783 delivery of sediment and its environmental implications, *Yangtze River*,
784 *Geophys. Res. Lett.*, 34(10), doi: 10.1029/2007GL029472, 2007.

785 Zhang, Q., Li, L., Wang, Y., Werner, A., Xin, P., Jiang, T., Barry, D.: Has the Three-
786 Gorges Dam made the Poyang Lake wetlands wetter and drier? *Geophys. Res.*
787 *Lett.*, 39(20), 28, doi: 10.1029/2012GL053431, 2012.

788 Zhang, S., Zhai, X., Yang, P., Xia, J., Hu, S., Zhou, L., Fu, C.: Ecological health
789 analysis of wetlands in the middle reaches of Yangtze River under changing

790 environment, *Int. J. Digit. Earth*, 16(1), 3125–3144, doi:
791 10.1080/17538947.2023.2244471, 2023.

792 Zhou, M., Xia, J., Deng, S., Shen, J., Mao, Y.: Modelling of phosphorus and
793 nonuniform sediment transport in the Middle Yangtze River with the effects of
794 channel erosion , tributary confluence and anthropogenic emission. *Water Res.*,
795 243, 120304, doi: 10.1016/j.watres.2023.120304. 2023.

796 Zhou, Y., Wang, Y., Li, Y., Zwahlen, F., Boillat, J.: Hydrogeochemical characteristics
797 of central Jiangnan Plain, China. *Environ. Earth Sci.*, 68(3), 765–778, doi:
798 10.1007/s12665-012-1778-9, 2013.

799